

## Tuning dissipation dilution in 2D material resonators by MEMS-induced tension

Wopereis, Michiel P.F.; Bouman, Niels; Dutta, Satadal; Steeneken, Peter G.; Alijani, Farbod; Verbiest, Gerard J.

**DOI**

[10.1063/5.0203122](https://doi.org/10.1063/5.0203122)

**Publication date**

2024

**Document Version**

Final published version

**Published in**

Journal of Applied Physics

**Citation (APA)**

Wopereis, M. P. F., Bouman, N., Dutta, S., Steeneken, P. G., Alijani, F., & Verbiest, G. J. (2024). Tuning dissipation dilution in 2D material resonators by MEMS-induced tension. *Journal of Applied Physics*, 136(1), Article 014302. <https://doi.org/10.1063/5.0203122>

**Important note**

To cite this publication, please use the final published version (if applicable).  
Please check the document version above.

**Copyright**

Other than for strictly personal use, it is not permitted to download, forward or distribute the text or part of it, without the consent of the author(s) and/or copyright holder(s), unless the work is under an open content license such as Creative Commons.








**Takedown policy**

Please contact us and provide details if you believe this document breaches copyrights.  
We will remove access to the work immediately and investigate your claim.

RESEARCH ARTICLE | JULY 02 2024

## Tuning dissipation dilution in 2D material resonators by MEMS-induced tension

Special Collection: [Two-Dimensional Materials and Heterostructures Under Strain](#)

Michiel P. F. Wopereis ; Niels Bouman ; Satadal Dutta ; Peter G. Steeneken ; Farbod Alijani ;  
Gerard J. Verbiest  



*J. Appl. Phys.* 136, 014302 (2024)

<https://doi.org/10.1063/5.0203122>



### Journal of Applied Physics

Special Topic:

Disordered Materials at the Atomic Scale

Guest Editors: Jaeyun Moon, Matteo Baggioli

[Submit Today!](#)




# Tuning dissipation dilution in 2D material resonators by MEMS-induced tension

Cite as: J. Appl. Phys. **136**, 014302 (2024); doi: [10.1063/5.0203122](https://doi.org/10.1063/5.0203122)

Submitted: 9 February 2024 · Accepted: 15 June 2024 ·

Published Online: 2 July 2024



Michiel P. F. Wopereis,  Niels Bouman,  Satadal Dutta,  Peter C. Steeneken,  Farbod Alijani,   
and Gerard J. Verbiest<sup>a)</sup> 

## AFFILIATIONS

Department of Precision and Microsystems Engineering, Delft University of Technology, Mekelweg 2, 2628 CD Delft, The Netherlands

**Note:** This paper is part of the special topic, Two-Dimensional Materials and Heterostructures Under Strain.

<sup>a)</sup>Author to whom correspondence should be addressed: [G.J.Verbiest@tudelft.nl](mailto:G.J.Verbiest@tudelft.nl)

## ABSTRACT

Resonators based on two-dimensional (2D) materials have exceptional properties for application as nanomechanical sensors, which allows them to operate at high frequencies with high sensitivity. However, their performance as nanomechanical sensors is currently limited by their low quality ( $Q$ )-factor. Here, we make use of micro-electromechanical systems (MEMS) to apply pure in-plane mechanical strain, enhancing both their resonance frequency and  $Q$ -factor. In contrast to earlier work, the 2D material resonators are fabricated on the MEMS actuators without any wet processing steps using a dry-transfer method. A platinum clamp, which is deposited by electron beam-induced deposition, is shown to be effective in fixing the 2D membrane to the MEMS and preventing slippage. By in-plane straining the membranes in a purely mechanical fashion, we increase the tensile energy, thereby diluting dissipation. This way, we show how dissipation dilution can increase the  $Q$ -factor of 2D material resonators by 91%. The presented MEMS actuated dissipation dilution method does not only pave the way toward higher  $Q$ -factors in resonators based on 2D materials, but also provides a route toward studies of the intrinsic loss mechanisms of 2D materials in the monolayer limit.

© 2024 Author(s). All article content, except where otherwise noted, is licensed under a Creative Commons Attribution (CC BY) license (<https://creativecommons.org/licenses/by/4.0/>). <https://doi.org/10.1063/5.0203122>

## I. INTRODUCTION

Nanomechanical resonators made of two-dimensional (2D) materials are the subject of intensive research due to their remarkable properties. Their low mass, combined with their high Young's modulus, leads to resonance frequencies that are typically a few tens of MHz.<sup>1</sup> Yet, their extreme flexibility in the out-of-plane direction enhances the sensitivity to external stimuli and makes them promising for various applications, including mass,<sup>1–4</sup> force,<sup>5–7</sup> pressure,<sup>6,8–11</sup> and temperature sensing.<sup>6,12,13</sup>

The performance of nanomechanical resonant sensors and clocks is generally limited by their dissipation per cycle ( $\Delta W$ ). A low  $\Delta W$  results in a high quality ( $Q$ )-factor, which is the ratio of stored energy  $W$  to  $\Delta W$  over a single oscillation cycle ( $Q = 2\pi W/\Delta W$ ). A low  $\Delta W$  and, thus, a high  $Q$ -factor physically insulates the resonator from external noise sources, allowing long-term coherent oscillations while minimizing energy dissipation to

the environment,<sup>14,15</sup> thus enabling low phase-noise oscillators<sup>16</sup> and high-performance noise-rejection filters.<sup>15,17,18</sup>

Increasing the tensile stress can be an effective strategy to realize high- $Q$  resonators.<sup>19,20</sup> The tension leads to an increase in the stored energy  $W$  without significantly affecting losses, thereby increasing the ratio  $W/\Delta W$  and the  $Q$ -factor,<sup>21</sup> an effect that is commonly known as dissipation dilution. Since this strategy was very successful in realizing high- $Q$  resonators in SiN that can be grown with high intrinsic tensile stress,<sup>20</sup> it was also considered as a method for increasing the quality factor of 2D materials that could not be grown with high intrinsic stress such that they might become serious contenders for high- $Q$  sensors and high  $f/Q$  resonant quantum devices. Out-of-plane electrostatic and thermal forces were used to achieve this quality factor tuning.<sup>22</sup> However, attempts to increase the  $Q$ -factor through out-of-plane electrostatic gating of 2D material membranes typically result in a reduction of the  $Q$ -factor instead of an increase by dissipation dilution.<sup>4,5,23</sup> This

16 JULY 2024 10:05:53

reduction is due to the voltage-dependent electronic Joule dissipation of the displacement current within the resonator.<sup>23,24</sup> Furthermore, the out-of-plane electrostatic pulling force increases sidewall adhesion, which facilitates dissipation through coupling with the substrate.<sup>22,25,26</sup> Thermal expansion-based tuning strategies to increase  $Q$ <sup>22</sup> have the drawback of making it difficult to distinguish tension effects from other thermal effects on  $Q$ . For example, the change in the membrane temperature changes material parameters that can increase damping via, e.g., the thermoelastic dissipation mechanism.<sup>15,27</sup>

Considering these drawbacks, it would be ideal to apply pure in-plane mechanical stress to increase the  $Q$  of 2D resonators. To reach this goal, special micro-electromechanical system (MEMS) actuators were developed in earlier works.<sup>28–30</sup> However, all these approaches have a step in which liquids, such as glues or etchants, are in contact with the 2D material, thereby affecting the device properties and  $Q$ . Moreover, the involved liquids and the complex fabrication process result in a low device yield, making it difficult to show the clamping efficiency of 2D materials on MEMS actuators. The field is, thus, in need of a simplified, dry fabrication method for MEMS actuators with integrated and clamped 2D materials.

In this paper, we achieve this goal and provide evidence of dissipation dilution in suspended 2D material resonators that are controllably tensioned in-plane using a micro-electromechanical systems (MEMS) actuator, as illustrated in Fig. 1. To enable these experiments, we introduce a dry-transfer method to precisely suspend 2D materials over MEMS gaps and rigidly clamp them with a layer of platinum using electron-beam-induced deposition (EBID). We actuate the membrane resonances optothermally and record the resulting motion using an interferometry setup, from which we extract the  $Q$ -factor ( $Q$ ) and the resonance frequency ( $f_0$ ). By applying strain with the MEMS actuator to the 2D material resonator in a mechanical and controllable fashion, we find an increase in the resonance frequency as well as the  $Q$ -factor, which are consistent with dissipation dilution. Our findings, thus, provide a new way for enhancing the  $Q$ -factor via dissipation dilution in 2D material resonators realized with a dry fabrication method.

## II. FABRICATION

We use a MEMS actuator that is designed and fabricated in the commercially available XMB10 process from X-FAB.<sup>31,32</sup> The resulting device (see Fig. 1) consists of a moving shuttle with 38 comb fingers that is held suspended by four serpentine flexures. The flexures are connected to fixed anchors that have aluminum bond pads for making electrical contact by wire bonding. The crystalline silicon shuttle has a thickness of  $15\text{ }\mu\text{m}$ , a length of  $520\text{ }\mu\text{m}$ , a comb finger length of  $103\text{ }\mu\text{m}$ , and an asymmetric finger spacing of  $2.0$  and  $4.0\text{ }\mu\text{m}$ . The membranes are suspended over a  $6\text{ }\mu\text{m}$  trench between the fixed anchor and the moving shuttle. Inside the trench, at a depth of  $5\text{ }\mu\text{m}$  below the shuttle surface, a suspended silicon beam acts as a mirror for interferometric readout of the membrane motion. In order to transfer the membranes onto the MEMS actuator, we first mechanically exfoliate 2D materials<sup>33</sup> onto a  $5 \times 5\text{ mm}^2$  PDMS sheet on a microscope slide. Next, we use a microscope to select membranes on the PDMS sheet with a minimum length of  $20\text{ }\mu\text{m}$  such that they can cover the suspended trench as well as parts of the fixed anchor and the moving shuttle. Membranes are selected based on their flatness and uniformity. Once we find a suitable membrane, we use a dome-shaped PDMS stamp covered with a sacrificial polypropylene carbonate (PPC) film on a microscope slide to pick it up from the PDMS sheet.<sup>34</sup> The utilization of a PDMS dome results in a smaller contact area with the MEMS actuator, approximately  $350\text{ }\mu\text{m}$  in diameter, which allows the precise positioning of a membrane using a manual transfer system of HQ2D while minimizing contaminations. The microscope slides ensure that we can see the flake during transfer and position it accurately. We then bring the membrane on the PDMS dome in contact with the MEMS actuator and heat the stage to  $110\text{ }^\circ\text{C}$  (above the melting point of PPC). This causes the PPC film to melt and ensures the transfer of the membrane onto the designated area [see Fig. 2(b)]. After the transfer, we wire bond the MEMS actuator and connect all terminals to a common ground; this crucial step prevents any electrostatic force-induced movement during the rest of the fabrication process. Next, we remove the PPC film from the membrane and the MEMS

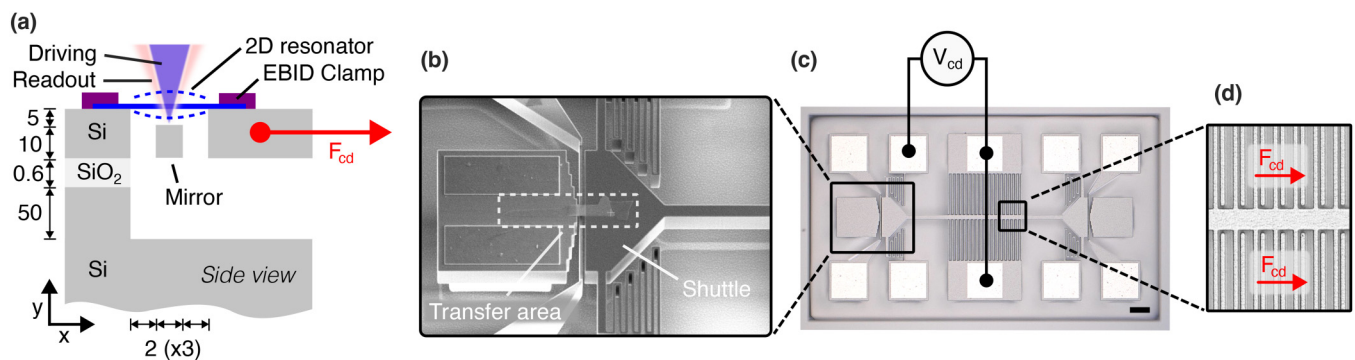


**FIG. 1.** Tunable 2D material resonator via MEMS-induced tension. (a) Side view of the final device illustrating the 2D material, EBID clamps, drive- and readout lasers, and the force  $F_{cd}$  induced by the MEMS actuator. Dimensions are in micrometers. (b) SEM image under an angle of the device. (c) Top view of an empty MEMS actuator. Scale bar:  $50\text{ }\mu\text{m}$ . Voltage over comb-drive fingers ( $V_{cd}$ ). (d) Detailed view of the comb drive indicating the direction of the comb-drive force ( $F_{cd}$ ).

16 July 2024 10:05:53

actuator through annealing in a high vacuum oven at a pressure below  $10^{-5}$  mbar for 3 h at a temperature of  $300^{\circ}\text{C}$  (exceeding the decomposition temperature of PPC<sup>35</sup>). After annealing, we inspect the sample optically to confirm the PPC removal [see Fig. 2(c)]. Finally, we clamp the membrane with a layer of platinum using EBID.<sup>36</sup> Other materials or composites for clamping might be considered as well for the ease of fabrication or enhancing the mechanical properties of the final device, e.g., by maximizing the stiffness of the clamps.<sup>37</sup> We used platinum as it was readily available and is chemically inert, yet compatible with EBID. Detailed information on the fabrication procedure is available in the [supplementary material S1](#).

In total, we fabricated four devices (D1–D4) with different 2D materials using the method outlined above (see Table I). Figure 1(a) shows a schematic cross section of a device, including the dimensions. All membranes have a suspended length of  $6\mu\text{m}$ , width  $w$ , and thickness  $t$ , as determined with a white light interferometer (see Table I).

To mechanically tension 2D materials with the MEMS actuators [see Figs. 1(b)–1(d)], we apply a potential difference  $V_{\text{cd}}$  between the comb fingers. Due to the asymmetric placement of the comb fingers [see Fig. 1(d)], a force  $F_{\text{cd}} = -\frac{1}{2}\frac{\partial C}{\partial x}V_{\text{cd}}^2$  will act on the moving shuttle and will tension the membrane and the four serpentine flexures. Here,  $\frac{\partial C}{\partial x}$  is the change in capacitance  $C$  between the comb fingers with respect to a change in position  $x$  of the moving shuttle.

Based on their geometry, the MEMS actuators used here can controllably strain membranes up to  $\approx 11\%$ , which is set by the maximum in-plane displacement of  $\approx 0.67\mu\text{m}$  ( $1/3$  of the  $2\mu\text{m}$

actuation gap) over a  $6\mu\text{m}$  suspended length. As the maximum in-plane displacement is the limiting factor, pre-deformations and wrinkles in 2D materials<sup>22,26,38</sup> can reduce the maximum achievable strain. Moreover, the bare MEMS actuator has a pull-in voltage of  $13.5 \pm 0.5$  V (see [supplementary material S2](#)). As a result, if the stiffness of the 2D membrane stiffness is low, e.g., because it is wrinkled, the MEMS actuator will collapse at this voltage. However, for certain devices, the stiffness of the 2D membrane was high such that it increased the total device stiffness significantly with respect to that of the MEMS springs and, as a consequence, led to an increase in the pull-in voltage. We were able to apply voltages up to 60 V for device D4 without a pull-in, which demonstrates that the force and stiffness provided by the 2D material were substantial.

### III. MEASUREMENTS

We measure the dynamics of the membranes using an optical interferometry setup [see Fig. 3(a)]. The devices are placed in a vacuum chamber with a pressure below  $10^{-5}$  mbar and are actuated using a blue diode laser ( $\lambda = 405$  nm) that is power-modulated through a vector network analyzer (VNA). We use a red He–Ne laser ( $\lambda = 632$  nm) to measure the motion of the membrane as its reflected intensity highly depends on the distance between the membrane and the mirror [see Fig. 3(b)]. The intensity of the reflected red laser light is detected using a photodiode and further processed by the VNA. Figure 3(c) shows a typical response recorded by the VNA. We observe multiple peaks in the spectrum that we identify as resonance frequencies. To analyze these further,

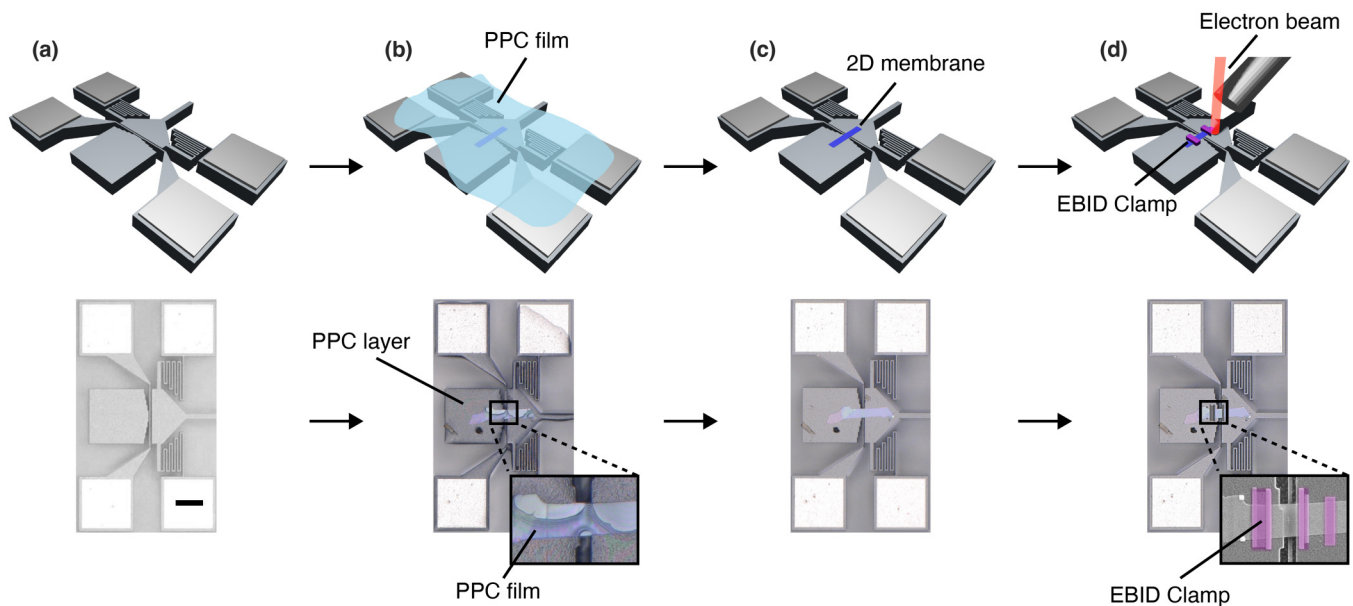


**FIG. 2.** Fabrication procedure: drawings, optical and SEM micrographs. (a) Device straining platform. Scale bar:  $50\mu\text{m}$ . (b) Device after the membrane transfer using a sacrificial PPC layer. (c) Device after annealing. (d) Illustration of the EBID process, an optical image of the device after clamping, and a false-colored SEM image highlighting the platinum clamps.

16 July 2024 10:05:53



**TABLE I.** Characteristics of fabricated devices D1–D4, including 2D material, clamped using EBID of platinum, width  $w$ , thickness  $t$ , and fitted parameters  $Q_{\text{int}}/f_{\text{plate}}^2$  and  $Q_{\text{ext}}$ , where  $Q_{\text{int}}$  is the intrinsic quality factor due to bending and elongation losses,  $f_{\text{plate}}$  is the resonance frequency due to the bending rigidity, and  $Q_{\text{ext}}$  is damping from extrinsic dissipation sources [see Eq. (3)]. The membrane thickness is determined using AFM. The width is obtained by measuring an optical or SEM image.

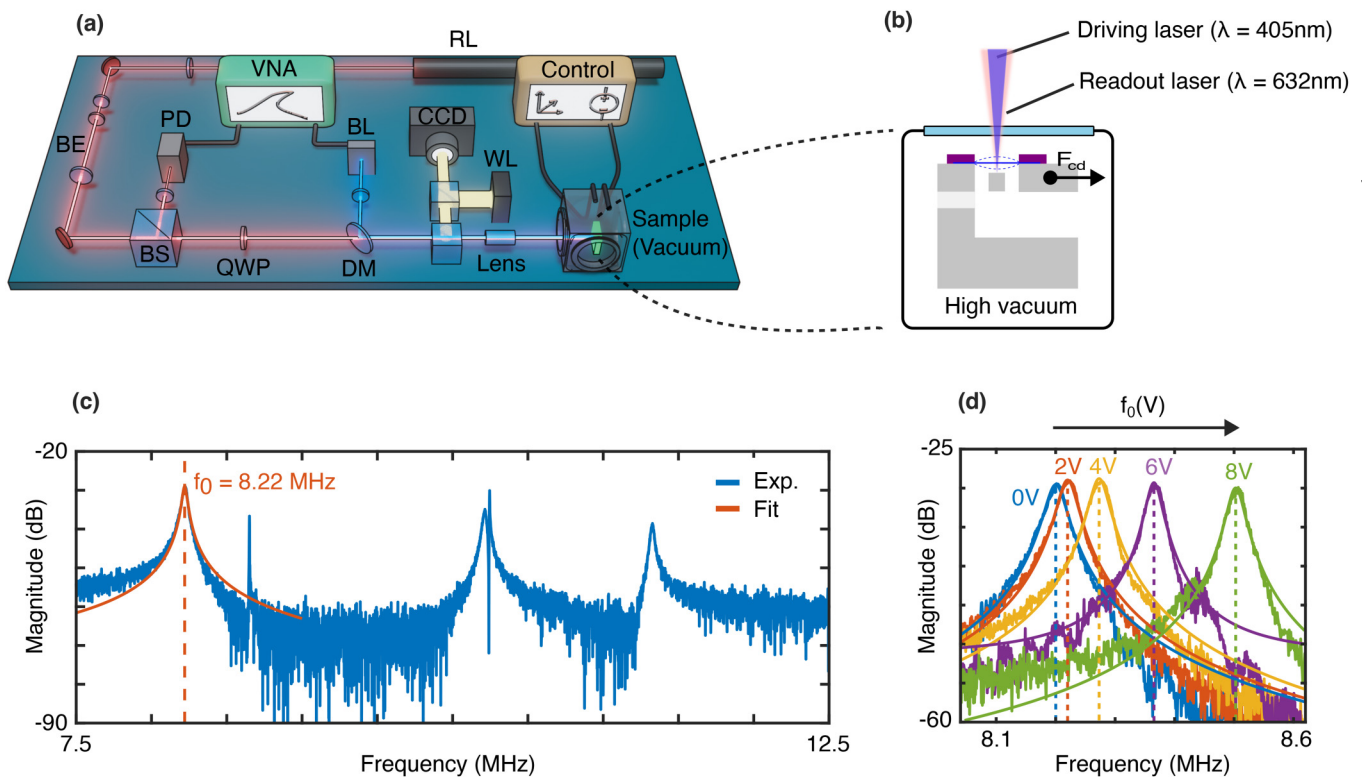
| Device | Material | Clamped | $w$ ( $\mu\text{m}$ ) | $t$ (nm)         | $Q_{\text{int}}/f_{\text{plate}}^2$ ( $\text{Hz}^{-2}$ ) | $Q_{\text{int}}$ | $Q_{\text{ext}}$ |
|--------|----------|---------|-----------------------|------------------|--|------------------|------------------|
| D1     | Graphene | No      | 7.2                   | $9.8 \pm 0.33$   | $7.084 \times 10^{-12}$                                  | <71              | 182              |
| D2     | Graphene | No      | 16.7                  | $22.47 \pm 0.15$ | $2.106 \times 10^{-12}$                                  | <127             | >1000            |
| D3     | MoS2     | Yes     | 19.9                  | $77.79 \pm 0.33$ | $1.362 \times 10^{-12}$                                  | <64              | 180              |
| D4     | WS2      | Yes     | 16.0                  | $94.39 \pm 0.23$ | $2.515 \times 10^{-12}$                                  | <203             | >1000            |

we fit the frequency response  $M$  of the fundamental resonance to the well-known harmonic oscillator model,<sup>15,39,40</sup>

$$M(f) = \frac{(Af^2/Q)}{\sqrt{(f_0^2 - f^2)^2 + \left(\frac{f_0 f}{Q}\right)^2}}, \quad (1)$$

where  $f_0$  is the resonance frequency in Hz,  $Q$  is the quality factor, and  $A$  is the peak amplitude. Figure 3(c) shows this fit on the

frequency response of device D4 at  $V_{\text{cd}} = 2$  V, from which we extract a resonance frequency of 8.22 MHz. We then repeat the measurement for different  $V_{\text{cd}}$  [see Fig. 3(d)] to analyze the dependence of  $f_0$  and  $Q$  on the applied force  $F_{\text{cd}}$ . As Fig. 3(d) shows, we see an increase in  $f_0$  with applied  $V_{\text{cd}}$  due to the increase in tension in the membrane. We observe a similar increase in the resonance frequency with applied  $V_{\text{cd}}$  for the higher mode between 11 and 12 MHz, as depicted in supplementary material S3.



16 July 2024 10:05:53

**FIG. 3.** Device measurements. (a) Fabry–Pérot interferometry setup for measuring the resonance frequencies. Vector Network Analyzer (VNA),  $V_{\text{cd}}$  and stage control (control), Beam expander (BE), Beam splitter (BS), Quarter wave plate (QWP), Dichroic mirror (DM), White light source (WL), Photodetector (PD), Red ( $\lambda = 632$  nm) He–Ne Laser (RL), and Blue ( $\lambda = 405$  nm) Diode Laser (BL). (b) Side view of the device inside the high vacuum chamber. (c) Fitting the harmonic oscillator equation on the experimental data of the VNA for device D4 at  $V_{\text{cd}} = 2$  V to extract the resonance frequency ( $f_0$ ) and the quality factor ( $Q$ ). (d) Experimental data of the VNA for device D4 for  $V_{\text{cd}} = 0, 2, 4, 6$ , and  $8$  V (DC).

## IV. CLAMPING OF 2D MATERIAL RESONATORS

To evaluate the effectiveness of a deposited layer of platinum using EBID in clamping 2D material resonators, we compare the response of an unclamped device (D1) to the response of a clamped one (D3). We vary the comb-drive force  $F_{cd}$  for both devices by varying  $V_{cd}$ . In a single sweep, we start at  $V_{cd} = 0$  V, increase the voltage to a maximum  $V_{max}$ , return to 0 V, decrease the voltage to  $-V_{max}$ , and finally return to 0 V. For each subsequent sweep, we increase  $V_{max}$  by 1 V up to a maximum of 5 V for device D1, to gradually increase the maximum force exerted on the membrane, and monitor the shift in the fundamental resonance. Figure 4 shows  $f_0$  as a function of  $V_{cd}$  extracted from one such experiment for devices D1 and D3. For the unclamped device [see Fig. 4(a)], we observe a significant decrease in  $f_0$  at  $V_{cd} = 0$  V after each voltage sweep. At the last measurement point at 0 V,  $f_0$  shows an irreversible reduction from 4.30 to 3.73 MHz, which corresponds to a decrease of approximately 13% with respect to the very first measurement on this membrane. The permanent reduction of  $f_0$  might be attributed to irreversible slippage, unsticking, or ironing out the wrinkles that increase the effective length of the membrane, reduce its tension, and, thus, resonance frequency. This is in contrast to recent observations of a reversible sliding scenario where a closed  $f_0$  vs  $V_{cd}$  loop is expected.<sup>43</sup>

In contrast to the unclamped device D1, device D3 contains a clamped membrane, as depicted in the inset of Fig. 4(b). As Fig. 4(b) shows, we observe a notably different  $f_0$  vs  $V_{cd}$  response when compared to the unclamped device. Initially,  $f_0$  measures 7.49 MHz, ascending to 13.67 MHz at 30 V, and decreasing back to 7.42 MHz at 0 V, a change of less than 1%. In subsequent sweeps, the resonance frequency at  $V_{cd} = 0$  V remains stable within a range of 0.02 MHz. These measurements show that the resonance frequency  $f_0$  of the device D3 is much more stable than that of the unclamped device, even at substantially higher actuation voltages, resulting in a 36 times larger force ( $F_{cd} \propto V_{cd}^2$ ) than applied in measurements on device D1. This difference between the clamped and unclamped devices indicates that the deposited layer of platinum using EBID is effective in

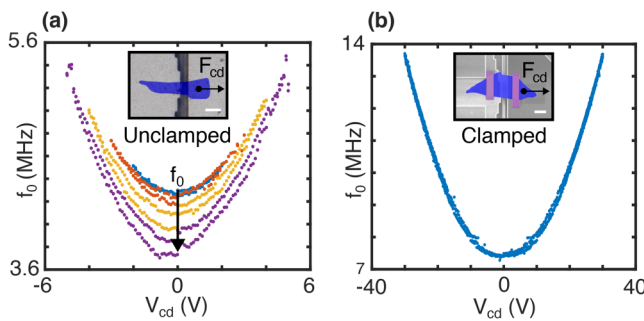


**FIG. 4.** Comparison of the resonance frequency ( $f_0$ ) vs the comb-drive voltage ( $V_{cd}$ ).  $F_{cd}$  indicates the pulling direction of the suspended shuttle by the comb-drive actuator. Scale bars: 10  $\mu$ m. (a) Unclamped device D1,  $V_{max} = 2$  V (blue), 3 V (orange), 4 V (yellow), and 5 V (purple), false-colored optical image (blue: 2D membrane) (b) Device D3 clamped with a platinum layer deposited by EBID,  $V_{max} = 30$  V (blue), false-colored SEM image (blue: 2D membrane, purple: platinum clamps).

preventing permanent tension reduction during MEMS actuation. Since the EBID clamps are separated by a few micrometers from the edge of the trench and, thus, cannot significantly affect unwrinkling and adhesion mechanisms inside the trench, we also conclude that the irreversible changes in  $f_0$  in Fig. 4(a) are most likely due to slippage of a large part of the flake over the silicon surface.

Furthermore, it is worth noting that the maximum voltage of 30 V significantly surpasses the pull-in voltage  $V_{PI}$  of the bare MEMS actuator, which was determined to be  $13.5 \pm 0.5$  V (see [supplementary material S2](#)), providing evidence that the clamped membrane generates a substantial force on the shuttle, thus preventing its pull-in and collapse. Simultaneously, according to Newton's third law, we conclude that the MEMS actuator effectively pulls and strains the clamped membranes. An equivalent observation for unclamped device D2 and clamped device D4 can be found in [supplementary material S4](#).

## V. DISSIPATION DILUTION

By fitting resonance peaks, such as in Fig. 3(d), we extract both the quality factor  $Q$  and resonance frequency  $f_0$ . To study the

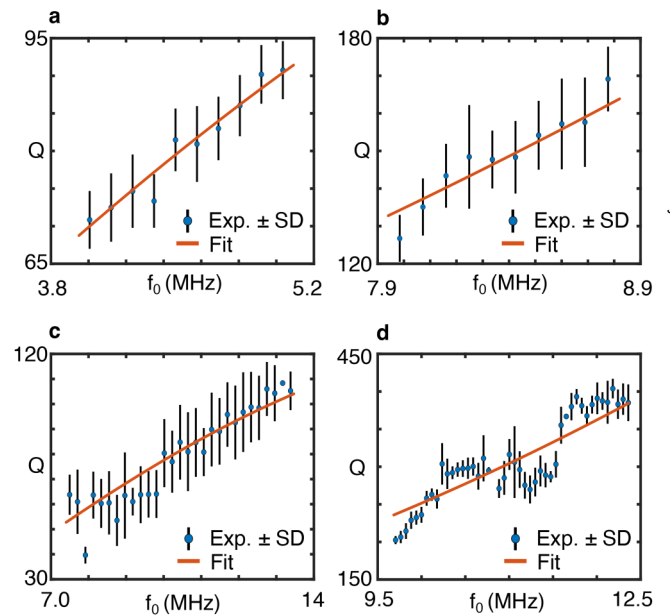


**FIG. 5.** Dissipation dilution in unclamped devices D1–D2 and clamped devices D3–D4. Quality factor ( $Q$ ) vs the resonance frequency ( $f_0$ ). The unclamped devices exhibit a decline in  $f_0$  and  $Q$  due to slippage, in contrast with the clamped devices, which show consistent values for  $f_0$  and  $Q$  at  $V_{cd} = 0$  V. (a) Experimental data from unclamped device D1 from the  $V_{max} = 4$  V-cycle. The device starts at  $f_0 = 4.17$  MHz and  $Q = 73.5$  and stops at  $f_0 = 3.96$  MHz and  $Q = 69.0$  due to slippage. (b) Experimental data from unclamped device D2 from the  $V_{max} = 12$  V-cycle. The device starts at  $f_0 = 8.45$  MHz and  $Q = 150$  and stops at  $f_0 = 7.95$  MHz and  $Q = 113$  due to slippage. (c) Experimental data of clamped device D3 from the  $V_{max} = 30$  V-cycle. The device maintains a consistent  $f_0$  and  $Q$  of 7.50 MHz and 63.8, respectively. (d) Experimental data of clamped device D4 from the  $V_{max} = 60$  V-cycle. The device maintains a consistent  $f_0$  and  $Q$  of 9.70 MHz and 202, respectively.

16 July 2024 10:05:53

effectiveness of the MEMS actuator in tuning the quality factor by dissipation dilution, we plot  $Q$  vs  $f_0$  for both unclamped and clamped devices over the full actuation voltage range in Fig. 5. It is seen that the  $Q$ -factor of all devices increases with  $f_0$ , as expected in a dissipation dilution scenario. For instance, device D4 experiences a 30% increase in  $f_0$  and a 91% increase in  $Q$ . Interestingly, despite the presence of slipping effects, this trend even seems to hold for the unclamped devices D1 and D2 shown in Figs. 5(a) and 5(b), respectively.

We now compare the experimental relation between  $f_0$  and  $Q$  with theory. From the literature,<sup>14</sup> the quality factor  $Q_D$  of a resonator in the presence of dissipation dilution is given by (see supplementary material S5)

$$Q_D \approx \left( \frac{f_0}{f_{\text{plate}}} \right)^2 Q_{\text{int}}, \quad (2)$$

where  $f_0$  is the measured resonance frequency,  $f_{\text{plate}}$  is the frequency in the presence of bending rigidity, and  $Q_{\text{int}}$  is the intrinsic dissipation. In the presence of other external dissipation mechanisms with quality factor  $Q_{\text{ext}}$ , the total  $Q$ -factor can be further reduced<sup>15,19</sup> to a value  $Q$ ,

$$\frac{1}{Q} = \frac{1}{Q_D} + \frac{1}{Q_{\text{ext}}}. \quad (3)$$

We fit Eq. (3) to the experimental data in Fig. 5 with  $Q_{\text{int}}/f_{\text{plate}}^2$  and  $Q_{\text{ext}}$  as fit parameters (orange lines). We provide the fitting values in Table I. Note that the fitted lines are almost linear because they span only a small frequency range. For the fit parameter  $Q_{\text{int}}/f_{\text{plate}}^2$ , we find a similar order of magnitude for all devices. As we assume that  $f_0$  equals  $f_{\text{plate}}$  when the membranes are unstrained ( $V_{\text{cd}} = 0$  V, see supplementary material S5), we estimate  $Q_{\text{int}}$  by multiplying  $Q_{\text{int}}/f_{\text{plate}}^2$  with  $f_0(0 \text{ V})^2$ . The large values of  $Q_{\text{int}}$  (see Table I) support the underpinning hypothesis of Eq. 2 that the storage modulus of these materials is much larger than their loss modulus. For devices D1 and D3, we fitted an extrinsic damping contribution of  $Q_{\text{ext}} \approx 180$ . For devices D2 and D4, the data could be fitted well without assuming an external dissipation source  $Q_{\text{ext}}$ , and therefore, we took  $1/Q_{\text{ext}} = 0$ . The good agreement between the experimental data and the fitted curves using Eq. (3) provides evidence that dissipation dilution can account for the observations.

## VI. DISCUSSION

In Secs. II–V, we studied the effect of in-plane stress on the  $Q$ -factor and the resonance frequency of membranes made of multi-layered 2D materials. The results show that the quality factor can be enhanced by generating tension on the 2D material membranes, and the obtained data match reasonably well with a dissipation dilution model. We note that this observation does not rule out other mechanisms that may affect the quality factors. These include (i) mode coupling to other modes of the membrane;<sup>44–46</sup> (ii) a change in dissipation rate  $\Delta W$  with applied tension;<sup>26,47,48</sup> (iii) changes in the membrane's geometry with increasing tension, which could be attributed to suppressing wrinkles;<sup>38,49</sup> (iv) the

release of edge adhesion during membrane straining,<sup>50</sup> which facilitates the transfer of energy from the resonating membrane to the substrate, leading to acoustic radiation losses;<sup>51</sup> or (v) material fatigue behavior of both the 2D material and the platinum clamps under repeated mechanical cycling. Future work could focus on systematically studying these effects as a function of applied tension.

The main advantage of using a MEMS actuator to apply the tension is that it provides a pure in-plane force, in contrast to thermal, electrostatic gating, or gas pressure-based approaches, where the force is accompanied by other effects that might modify  $Q$ . The presented method also has some limitations. First of all, actuator device fabrication, design, and wire bonding are time-consuming. Moreover, the actuation range is limited to 1/3 of the actuator gap, although other actuator designs can provide a more extensive range. Finally, transferring membranes to a movable shuttle is a complicated task and can affect membrane suspending and adhesion to the MEMS actuator.

A key prospect of the presented work is the ability to apply MEMS tensioning to significantly raise the quality factor of 2D materials, with the aim to eventually scale it down to the monolayer limit and outperform record silicon nitride/carbide devices.<sup>52–54</sup> Although currently,  $Q$ s of 2D materials seem to be limited by their low stress and by fabrication artifacts, such as wrinkles, in the monolayer limit, the intrinsic  $Q_{\text{int}}$  of 2D materials might be much higher than that of multilayer materials since interlayer dissipation mechanisms and thermoelastic damping are largely eliminated.<sup>55</sup> Moreover, for sensing applications, such as resonant mass sensors, the large aspect ratio and low mass of 2D materials can increase sensitivity. In this respect, the high ultimate tensile stress of 2D materials, such as graphene, which was demonstrated to exceed 10 GPa,<sup>56</sup> can potentially outperform the tension limitations of even silicon carbides.<sup>52</sup>

Moreover, it is of interest to evaluate the minimum measured  $Q$  in more detail. For device D4, we found a  $Q$  of 202. Disregarding the small effect of pre-stress, we expect this  $Q$  to be roughly equal to the intrinsic  $Q$  since the thickness of the membrane is relatively high and the intrinsic  $Q$  is primarily governed by the bending contribution. This intrinsic  $Q$  is over 32 times lower than that of silicon nitride, for which a value of  $69t \text{ nm}^{-1}$  was found,<sup>57</sup> which for a thickness equal to that of device D4 of 94.39 nm evaluates to  $Q_{\text{int}} = 6513$ . A question for further study is if the low intrinsic  $Q$  in device D4 is due to the intrinsic crystal properties of  $\text{WS}_2$  compared to SiN or if the value is limited by imperfections, such as wrinkles. It is clear that the MEMS implementation of dissipation dilution demonstrated in this work, which results in  $Q$  enhancement up to 91%, is only a first step toward  $Q$ -factor engineering of 2D materials and by no means is yet as efficient as that in SiN resonators, where  $Q/Q_{\text{int}}$  factors of over  $10^4$  are reached.<sup>53</sup>

## VII. CONCLUSION

To conclude, we show signatures of dissipation dilution in 2D material resonators. We use a MEMS actuator to strain the membrane uniaxially and, thus, tune the resonance frequency and the  $Q$ -factor. To induce dissipation dilution, we developed a device fabrication method using dry transfer of membranes on the MEMS

16 JULY 2024 10:05:53



actuator and a clamping technique using EBID of platinum to prevent edge-slippage. The MEMS platform can also be used to study slipping and sliding effects, where slipping was observed to reduce both the  $Q$ -factor and  $f_0$ , in line with the dissipation dilution mechanism that increases  $Q$  with the MEMS actuation force. By pulling on the membranes, we control the in-plane tension of the membranes, which resulted in an increase in resonance frequency  $f_0$  of 30% and an accompanying increase of 91% in the  $Q$  factor. Our results enable a leap in developing higher- $Q$  resonators based on 2D materials with potential applications in sensing, time-keeping, and information processing.

## SUPPLEMENTARY MATERIAL

See the [supplementary material](#) for detailed fabrication instructions (S1), MEMS stiffness characterization (S2), frequency tuning of a higher mode (S3),  $f_0$  vs  $V$  measurements for devices D2 and D4 (S4), and derivation of the dissipation dilution model (S5).

## ACKNOWLEDGMENTS

We would like to thank the Plantenna Research Program funded by the 4TU Federation, the European Union's Horizon 2020 Research and Innovation Program under ERC Consolidator Grant NCANTO (No. 101125458) for financial support, and Europractice for providing the design tools and multi-project wafer service.

## AUTHOR DECLARATIONS

### Conflict of Interest

The authors have no conflicts to disclose.

## Author Contributions

**Michiel P. F. Wopereis:** Data curation (equal); Formal analysis (equal); Investigation (equal); Methodology (equal); Writing – original draft (equal); Writing – review & editing (equal). **Niels Bouman:** Conceptualization (equal); Data curation (equal); Formal analysis (equal); Investigation (equal); Methodology (equal). **Satadal Dutta:** Conceptualization (equal); Funding acquisition (equal). **Peter G. Steeneken:** Conceptualization (equal); Data curation (equal); Funding acquisition (equal); Supervision (equal); Writing – original draft (equal); Writing – review & editing (equal). **Farbod Alijani:** Conceptualization (equal); Data curation (equal); Supervision (equal); Writing – original draft (equal); Writing – review & editing (equal). **Gerard J. Verbiest:** Conceptualization (equal); Data curation (equal); Funding acquisition (equal); Supervision (equal); Visualization (equal); Writing – original draft (equal); Writing – review & editing (equal).

## DATA AVAILABILITY

The data that support the findings of this study are available from the corresponding author upon reasonable request.

## REFERENCES

- <sup>1</sup>A. Sakhaee-Pour, M. T. Ahmadian, and A. Vafai, "Applications of single-layered graphene sheets as mass sensors and atomistic dust detectors," *Solid State Commun.* **145**, 168 (2008).
- <sup>2</sup>B. Lassagne, D. Garcia-Sanchez, A. Aguiasca, and A. Bachtold, "Ultrasensitive mass sensing with a nanotube electromechanical resonator," *Nano Lett.* **8**, 3735 (2008).
- <sup>3</sup>J. Atalaya, J. M. Kinnaret, and A. Isacsson, "Nanomechanical mass measurement using nonlinear response of a graphene membrane," *Europhys. Lett.* **91**, 48001 (2010).
- <sup>4</sup>V. Singh, S. Sengupta, H. S. Solanki, R. Dhall, A. Allain, S. Dhara, P. Pant, and M. M. Deshmukh, "Probing thermal expansion of graphene and modal dispersion at low-temperature using graphene nanoelectromechanical systems resonators," *Nanotechnology* **21**, 165204 (2010).
- <sup>5</sup>P. Weber, J. Guttinger, A. Noury, J. Vergara-Cruz, and A. Bachtold, "Force sensitivity of multilayer graphene optomechanical devices," *Nat. Commun.* **7**, 12496 (2016).
- <sup>6</sup>M. C. Lemme, S. Wagner, K. Lee, X. Fan, G. J. Verbiest, S. Wittmann, S. Lukas, R. J. Dolleman, F. Niklaus, H. S. J. van der Zant, G. S. Duesberg, and P. G. Steeneken, "Nanoelectromechanical sensors based on suspended 2D materials," *Research* **2020**, 8748602.
- <sup>7</sup>I. E. Roslón, A. Japaridze, P. G. Steeneken, C. Dekker, and F. Alijani, "Probing nanomotion of single bacteria with graphene drums," *Nat. Nanotechnol.* **17**, 637 (2022).
- <sup>8</sup>J. Romijn, S. Vollebregt, R. J. Dolleman, M. Singh, H. S. Van Der Zant, P. G. Steeneken, and P. M. Sarro, "A miniaturized low power Pirani pressure sensor based on suspended graphene," in *2018 IEEE 13th Annual International Conference on Nano/Micro Engineered and Molecular Systems (NEMS)* (IEEE, 2018).
- <sup>9</sup>R. J. Dolleman, D. Davidovikj, S. J. Cartamil-Bueno, H. S. J. Van Der Zant, and P. G. Steeneken, "Graphene squeeze-film pressure sensors," *Nano Lett.* **16**, 568 (2016).
- <sup>10</sup>D. Shahdeo, A. Roberts, N. Abbineni, and S. Gandhi, "Graphene based sensors," in *Analytical Applications of Graphene for Comprehensive Analytical Chemistry*, Comprehensive Analytical Chemistry (Elsevier, 2020) pp. 175–199.
- <sup>11</sup>J. H. Choi, J. Lee, M. Byeon, T. E. Hong, H. Park, and C. Y. Lee, "Graphene-based gas sensors with high sensitivity and minimal sensor-to-sensor variation," *ACS Appl. Nano Mater.* **3**, 2257 (2020).
- <sup>12</sup>R. J. Dolleman, G. J. Verbiest, Y. M. Blanter, H. S. J. Van Der Zant, and P. G. Steeneken, "Nonequilibrium thermodynamics of acoustic phonons in suspended graphene," *Phys. Rev. Res.* **2**, 012058 (2020).
- <sup>13</sup>H. Liu, et al., "Enhanced photothermal response near the buckling bifurcation in 2d nanomechanical resonators," *2D Mater.* **11**, 025028 (2023).
- <sup>14</sup>L. Sementilli, E. Romero, and W. P. Bowen, "Nanomechanical dissipation and strain engineering," *Adv. Funct. Mater.* **32**, 2105247 (2022).
- <sup>15</sup>J. M. L. Miller, A. Ansari, D. B. Heinz, Y. Chen, I. B. Flader, D. D. Shin, L. G. Villanueva, and T. W. Kenny, "Effective quality factor tuning mechanisms in micromechanical resonators," *Appl. Phys. Rev.* **5**, 041307 (2018).
- <sup>16</sup>D. Leeson, "A simple model of feedback oscillator noise spectrum," *Proc. IEEE* **54**, 329 (1966).
- <sup>17</sup>T. B. Gabrielson, "Fundamental noise limits for miniature acoustic and vibration sensors," *J. Vib. Acoust.* **117**, 405 (1995).
- <sup>18</sup>T. Gabrielson, "Mechanical-thermal noise in micromachined acoustic and vibration sensors," *IEEE Trans. Electron Devices* **40**, 903 (1993).
- <sup>19</sup>S. Schmid, *Fundamentals of Nanomechanical Resonators* (Springer, 2016).
- <sup>20</sup>S. S. Verbridge, J. M. Parpia, R. B. Reichenbach, L. M. Bellan, and H. G. Craighead, "High quality factor resonance at room temperature with nanostrings under high tensile stress," *J. Appl. Phys.* **99**, 124304 (2006).
- <sup>21</sup>S. A. Fedorov, N. J. Engelsen, A. H. Ghadimi, M. J. Beryhi, R. Schilling, D. J. Wilson, and T. J. Kippenberg, "Generalized dissipation dilution in strained mechanical resonators," *Phys. Rev. B* **99**, 054107 (2019).
- <sup>22</sup>D. Davidovikj, M. Poot, S. J. Cartamil-Bueno, H. S. J. Van Der Zant, and P. G. Steeneken, "On-chip heaters for tension tuning of graphene nanodrums," *Nano Lett.* **18**, 2852 (2018).

16 JULY 2024 10:05:53

- <sup>23</sup>N. Morell, A. Reserbat-Plantey, I. Tsioutsios, K. G. Schädler, F. Dubin, F. H. L. Koppens, and A. Bachtold, "High quality factor mechanical resonators based on WSe<sub>2</sub> monolayers," *Nano Lett.* **16**, 5102 (2016).
- <sup>24</sup>X. Song, M. Oksanen, M. A. Sillanpää, H. G. Craighead, J. M. Parpia, and P. J. Hakonen, "Stamp transferred suspended graphene mechanical resonators for radio frequency electrical readout," *Nano Lett.* **12**, 198 (2012).
- <sup>25</sup>J. Rieger, A. Isacsson, M. J. Seitner, J. P. Kotthaus, and E. M. Weig, "Energy losses of nanomechanical resonators induced by atomic force microscopy-controlled mechanical impedance mismatching," *Nat. Commun.* **5**, 3345 (2014).
- <sup>26</sup>P. G. Steeneken, R. J. Dolleman, D. Davidovikj, F. Alijani, and H. S. J. van der Zant, "Dynamics of 2D material membranes," *2D Mater.* **8**, 042001 (2021).
- <sup>27</sup>R. Lifshitz and M. L. Roukes, "Thermoelastic damping in micro- and nanomechanical systems," *Phys. Rev. B* **61**, 5600 (2000).
- <sup>28</sup>G. J. Verbiest, D. Xu, M. Goldsche, T. Khodkov, S. Barzanjeh, N. Von Den Driesch, D. Buca, and C. Stampfer, "Tunable mechanical coupling between driven microelectromechanical resonators," *Appl. Phys. Lett.* **109**, 143507 (2016).
- <sup>29</sup>H. H. Perez-Garza, E. W. Kievit, G. F. Schneider, and U. Staufer, "Highly strained graphene samples of varying thickness and comparison of their behaviour," *Nanotechnology* **25**, 465708 (2014).
- <sup>30</sup>Y. Xie, J. Lee, Y. Wang, and P. X. Feng, "Straining and tuning atomic layer nanoelectromechanical resonators via comb-drive MEMS actuators," *Adv. Mater. Technol.* **6**, 2000794 (2021).
- <sup>31</sup>X. Zou, S. Ahmed, N. Jaber, and H. Fariborzi, "A compact high-sensitivity temperature sensor using an encapsulated clamped-clamped MEMS beam resonator," in *2021 21st International Conference on Solid-State Sensors, Actuators and Microsystems (Transducers)* (IEEE, 2021).
- <sup>32</sup>P. Streit, R. Forke, S. Voigt, U. Schwarz, R. Ziegenhardt, S. Weidlich, D. Billep, M. Gaitzsch, and H. Kuhn, "Vibration sensors with a high bandwidth and low SNR, enhanced with post processing gap reduction," in *2022 23rd International Conference on Thermal, Mechanical and Multi-Physics Simulation and Experiments in Microelectronics and Microsystems (EuroSimE)* (IEEE, 2022).
- <sup>33</sup>K. S. Novoselov, D. Jiang, F. Schedin, T. J. Booth, V. V. Khotkevich, S. V. Morozov, and A. K. Geim, "Two-dimensional atomic crystals," *Proc. Natl. Acad. Sci. U.S.A.* **102**, 10451 (2005).
- <sup>34</sup>K. Kinoshita, R. Moriya, M. Onodera, Y. Wakafuji, S. Masubuchi, K. Watanabe, T. Taniguchi, and T. Machida, "Dry release transfer of graphene and few-layer h-bn by utilizing thermoplasticity of polypropylene carbonate," *npj 2D Mater. Appl.* **3**, 22 (2019).
- <sup>35</sup>S. Wang, Y. Huang, B. Liao, G. Lin, G. Cong, and L. Chen, "Structure and properties of poly(propylene carbonate)," *Int. J. Polym. Anal. Charact.* **3**, 131 (1997).
- <sup>36</sup>M. Lee, D. Davidovikj, B. Sajadi, M. Siskins, F. Alijani, H. S. J. van der Zant, and P. G. Steeneken, "Sealing graphene nanodrums," *Nano Lett.* **19**, 5313 (2019).
- <sup>37</sup>M. Goldsche, G. J. Verbiest, T. Khodkov, J. Sonntag, N. V. D. Driesch, D. Buca, and C. Stampfer, "Fabrication of comb-drive actuators for straining nanostructured suspended graphene," *Nanotechnology* **29**, 375301 (2018).
- <sup>38</sup>R. J. Nicholl, H. J. Conley, N. V. Lavrik, I. Vlassiuk, Y. S. Puzyrev, V. P. Sreenivas, S. T. Pantelides, and K. I. Bolotin, "The effect of intrinsic crumpling on the mechanics of free-standing graphene," *Nat. Commun.* **6**, 8789 (2015).
- <sup>39</sup>R. M. Schmidt, G. Schitter, and A. Rankers, *The Design of High Performance Mechatronics: High-Tech Functionality by Multidisciplinary System Integration* (IOS Press, 2020).
- <sup>40</sup>R. S. Figliola and D. E. Beasley, *Theory and Design for Mechanical Measurements* (John Wiley & Sons, 2014).
- <sup>41</sup>G. J. Verbiest, M. Goldsche, J. Sonntag, T. Khodkov, N. von den Driesch, D. Buca, and C. Stampfer, "Tunable coupling of two mechanical resonators by a graphene membrane," *2D Mater.* **8**, 035039 (2021).
- <sup>42</sup>J. Sonntag, M. Goldsche, T. Khodkov, G. Verbiest, S. Reichardt, N. V. Den Driesch, D. Buca, and C. Stampfer, "Engineering tunable strain fields in suspended graphene by microelectromechanical systems," in *2019 20th International Conference on Solid-State Sensors, Actuators and Microsystems & Eurosensors XXXIII (TRANSDUCERS & EUROSensors XXXIII)* (IEEE, 2019).
- <sup>43</sup>Y. Ying, Z.-Z. Zhang, J. Moser, Z.-J. Su, X.-X. Song, and G.-P. Guo, "Sliding nanomechanical resonators," *Nat. Commun.* **13**, 6392 (2022).
- <sup>44</sup>X. Wang, D. Zhu, X. Yang, L. Yuan, H. Li, J. Wang, M. Chen, G. Deng, W. Liang, Q. Li, S. Fan, G. Guo, and K. Jiang, "Stressed carbon nanotube devices for high tunability, high quality factor, single mode GHz resonators," *Nano Res.* **11**, 5812 (2018).
- <sup>45</sup>A. Keşkekler, O. Shoshani, M. Lee, H. S. J. Van Der Zant, P. G. Steeneken, and F. Alijani, "Tuning nonlinear damping in graphene nanoresonators by parametric-direct internal resonance," *Nat. Commun.* **12**, 1099 (2021).
- <sup>46</sup>A. Keşkekler, V. Bos, A. M. Aragón, P. G. Steeneken, and F. Alijani, "Multimode nonlinear dynamics of graphene resonators," *Phys. Rev. Appl.* **20**, 064020 (2023).
- <sup>47</sup>C. Zener, "Internal friction in solids. I. Theory of internal friction in reeds," *Phys. Rev.* **52**, 230 (1937).
- <sup>48</sup>S. Schmid, K. D. Jensen, K. H. Nielsen, and A. Boisen, "Damping mechanisms in high-q micro and nanomechanical string resonators," *Phys. Rev. B* **84**, 165307 (2011).
- <sup>49</sup>R. J. Nicholl, N. V. Lavrik, I. Vlassiuk, B. R. Srijanto, and K. I. Bolotin, "Hidden area and mechanical nonlinearities in freestanding graphene," *Phys. Rev. Lett.* **118**, 266101 (2017).
- <sup>50</sup>R. J. Dolleman, Y. M. Blanter, H. S. J. Van Der Zant, P. G. Steeneken, and G. J. Verbiest, "Phonon scattering at kinks in suspended graphene," *Phys. Rev. B* **101**, 115411 (2020).
- <sup>51</sup>P. Steeneken, J. Ruigrok, S. Kang, J. Van Beek, J. Bontemps, and J.-J. Koning, "Parameter extraction and support-loss in MEMS resonators," *arXiv:1304.7953* (2013).
- <sup>52</sup>M. Xu, D. Shin, P. M. Sberna, R. Van Der Kolk, A. Cupertino, M. A. Bessa, and R. A. Norte, "High-strength amorphous silicon carbide for nanomechanics," *Adv. Mater.* **36**, 2306513 (2023).
- <sup>53</sup>D. Shin, A. Cupertino, M. H. J. de Jong, P. G. Steeneken, M. A. Bessa, and R. A. Norte, "Spiderweb nanomechanical resonators via Bayesian optimization: Inspired by nature and guided by machine learning," *Adv. Mater.* **34**, 2106248 (2022).
- <sup>54</sup>A. Cupertino, D. Shin, L. Guo, P. G. Steeneken, M. Bessa, and R. Norte, *Centimeter-scale Nanomechanical Resonators with low Dissipation* (2023).
- <sup>55</sup>N. Lindahl, D. Midtvedt, J. Svensson, O. A. Nerushev, N. Lindvall, A. Isacsson, and E. E. B. Campbell, "Determination of the bending rigidity of graphene via electrostatic actuation of buckled membranes," *Nano Lett.* **12**, 3526 (2012).
- <sup>56</sup>M. Goldsche, J. Sonntag, T. Khodkov, G. J. Verbiest, S. Reichardt, C. Neumann, T. Ouaj, N. Von Den Driesch, D. Buca, and C. Stampfer, "Tailoring mechanically tunable strain fields in graphene," *Nano Lett.* **18**, 1707 (2018).
- <sup>57</sup>L. Villanueva and S. Schmid, "Evidence of surface loss as ubiquitous limiting damping mechanism in SiN micro- and nanomechanical resonators," *Phys. Rev. Lett.* **113**, 227201 (2014).